OCEAN
ISSN 3008-1203

Open Access
Research Article

Wave-energy extraction by an articulated floating-plate wave-energy converter

Hui Liang[1], Hao Chen[2], and Siming Zheng[3,4] ✉

[1] *Technology Centre for Offshore and Marine, Singapore (TCOMS), 118411, Singapore*
[2] *Faculty of Science, Agriculture and Engineering, Newcastle University, Newcastle Upon Tyne, NE1 7RU, United Kingdom*
[3] *State Key Laboratory of Ocean Sensing & Ocean College, Zhejiang University, Zhoushan 316021, China*
[4] *School of Engineering, Computing and Mathematics, University of Plymouth, Plymouth, PL4 8AA, UK*

Cite This: *Ocean*, **2026**, *2*, 9470020

Read Online

ABSTRACT: This study investigates the hydrodynamic performance and wave-energy extraction capabilities of an articulated floating-plate wave-energy converter (WEC) consisting of multiple hinged segments. Using linear potential flow theory and the boundary-element method, we solve the boundary-value problem in two equivalent formulations: velocity potential and hydrodynamic pressure. The articulated structure is modeled using generalized modes that capture relative rotations at the hinges. For power absorption, we assume a linear power take-off (PTO) system at each hinge and analytically derive the optimal absorbed power in two-segment configurations. To demonstrate the accuracy of the implementation, the numerical results are validated against experimental data of a single plate and benchmark solutions for hinged systems. The results reveal a strong dependence of optimal capture efficiency on the hinge position of two-segment plates, with peak values exceeding unity when the hinge is shifted toward the upwave side following the zero-crossing locus of the imaginary part of the intrinsic admittance. Therefore, the hinge must be appropriately placed for maximizing the energy extraction in raft-type WECs.

KEYWORDS: wave-energy converter, articulated floating plate, generalized modes, boundary-element method, power take-off optimization

1 Introduction

Wave energy is a promising renewable energy resource owing to its high energy density, strong predictability, and widespread availability across global coastlines [1–3]. Being less seasonally variable and more temporally consistent than other renewable energy sources such as solar and wind, wave energy is an attractive candidate for reliable, continuous power generation [4]. Over the past few decades, attenuator-type devices have emerged as diverse wave-energy converters (WECs) with high power-capture capability and suitability to large-scale offshore deployment. These devices are typically aligned parallel to the direction of wave propagation, where they can effectively "ride" the waves, with their principal axis perpendicular to the wavefront [5]. From a power-capture perspective, attenuator WECs are classified into two main types: hinged-float-based devices and flexible-tube-based devices, each employing a different energy-conversion mechanism [6].

Hinged-float-based attenuators, often referred to as "raft"-type devices, comprise a series of semi-submerged articulated floaters. Wave action induces a relative pitch motion between the floaters, which is converted into useful energy via a power take-off (PTO) system, usually located at the connecting hinges. Typical historical and contemporary prototypes include the Cockerell raft [7], the McCabe wave pump [8], and the Pelamis [9], which reached a high level of technological readiness but remained commercially challenging. Other examples are DEXA [10], Seapower Platform [11], and the M4 device [12], which explores multi-float configurations with the optimized geometry and float sizes to broaden the wave-frequency spectrum of effective power capture. The more recent Mocean energy device [13] analyzes unique shape designs that both improve the performance of the device and enhance its survivability in large waves.

In contrast, flexible-tube-based attenuators, also known as "bulge wave" devices, utilize a fully submerged, water-filled flexible tube. A passing wave generates a pressure wave, or "bulge", that propagates along the tube. This internal bulge wave is then harnessed to drive a turbine at the device's end, consistent with the Anaconda concept [14], or is captured by a distributed PTO system, such as the electroactive polymers employed in the WEC S3 prototype [15]. Whereas hinged-float attenuators have been widely prototyped, flexible-tube-based devices remain in an earlier developmental stage owing to the difficulties of implementing effective control systems and designing durable, manufacturable materials.

The dynamics of attenuator WECs in waves (particularly those of hinged-float-based WECs) have been extensively evaluated in theoretical and numerical simulation studies. Many of these efforts aimed to optimize the energy-capture characteristics of attenuator-based WEC systems. The two-raft WEC is a long-standing foundational model for understanding the inherent complex hydrodynamics and optimization challenges of attenuator-based WECs. Applying the wave radiation–diffraction method in both the

Received: November 30, 2025; **Revised:** February 3, 2026
Accepted: February 14, 2026

✉Address correspondence to Siming Zheng, siming.zheng@zju.edu.cn

time and frequency domains, Zheng et al. [16] conducted a dynamic analysis of a two-raft wave-energy conversion device. They determined the influences of the key parameters (cylindrical raft length, axis ratio of the elliptical cross-section, PTO damping coefficients, and others) on the wave-energy capture factor. Jin et al. [17] and Han et al. [18] evaluated the dynamics and energy-capture performances of two-body raft WECs using the open-source time-domain simulation tool WEC-Sim, developed by the National Renewable Energy Laboratory and Sandia National Laboratories in 2014. Their numerical work was complemented with physical experimental results. In addition, a deep operator learning model called DeepONet accurately captures the WEC dynamics after training on the experimental data of a hinged-raft WEC [19].

Maximizing the power absorption in two-float wave energy systems has also garnered considerable interest. Early theory established that the maximum power is determined by the difference between the wave excitation power and radiated power [20]. However, these ideal conditions tend to translate into complex, unrealizsable PTO systems rather than into practical designs. A more practical optimization method theoretically isolates the PTO parameters and predicts the maximum absorption using unitary transformations and block matrix inversion, while accounting for relative pitch-motion constraints [21]. Subsequent research has expanded beyond identical floats into more realistic scenarios, investigating the impacts of float length ratios [22] and structural flexibility [23]. PTO modeling has also evolved from simple linear dampers to sophisticated representations of nonlinear hydraulic systems consisting of a nonlinear column damper [16] and a nonlinear stiffness mechanism with passive phase-control strategies, providing efficient operation across varying sea states [24]. Underpinning these advances are high-fidelity computational tools such as computational fluid dynamics, which capture nonlinear effects and validate system hydrodynamics [25,26].

Recent trends have shifted toward more integrated and intelligent approaches. For example, wave-to-wire modeling frameworks couple hydrodynamic, mechanical, and electrical dynamics for a more holistic system analysis [27]. Machine learning is increasingly being applied to power prediction [28] and advanced control strategies such as declutching and latching control [29] enable dynamic optimization of energy capture. Moreover, the research scope has broadened from isolated WECs to multi-purpose structures, such as hybrid WEC-breakwaters [26] and arrays of multiple hinged modules [30], indicating the progression of this field toward practical, large-scale deployment.

Employing the generalized mode technique, we here investigate the wave power absorption of an articulated floating plate, a model design of hinged modular solar farms. Traditionally, such hinged structures are modeled using the Lagrange multiplier technique, which treats each float as an independent unit constrained at the joints (e.g., see Refs. [16,17,23]). This method, however, incurs relatively high computational costs that escalate with increasing number of floats. More efficiently, the generalized mode technique models the entire assembly as a single structure, capturing the relative motion between adjacent floats through a series of generalized nodes. This approach predicts the system's dynamic response and power absorption characteristics with sufficient accuracy within a substantially reduced computational time.

The remainder of this paper is organized as follows. Section 2 presents the problem statement and the boundary-value problem. Section 3 details the hydrodynamic analysis, including the boundary element method with the free-surface Green function and the two equivalent integral-equation formulations (potential and pressure forms), and the generalized-mode treatment of articulated bodies. Section 4 derives the expressions for wave-energy extraction, PTO modeling, the optimal damping condition, and the non-dimensional absorbed power. Section 5 validates the numerical implementation on both single and hinged plates, and thoroughly discusses the influence of hinge position on the optimal power absorption of two-segment rectangular plates. Finally, Section 6 summarizes the key findings and presents recommendations for future work.

2 Statement of the problem

Consider a series of N floating plates connected by hinges and subjected to incident ocean waves. We define a three-dimensional coordinate system $Oxyz$ in which the Oxy plane coincides with the undisturbed free surface and the Oz axis points positively upward. Each pair of adjacent plates is joined by a hinge located at $x = X_n$ where $n = 1, 2, \ldots, N-1$, as illustrated in Fig. 1. The horizontal extent of the structure is defined as

$$\mathcal{P} = \bigcup_{n=1}^{N} \mathcal{P}_n \quad \mathcal{P}_n = \{(x,y) | X_{n-1} \le x \le X_n; -B_n \le y \le B_n\}, \tag{1}$$

with B_n defined as a function of $x \in [X_{n-1}, X_n]$, written as

$$B_n = \frac{b_n - b_{n-1}}{X_n - X_{n-1}} x - \frac{b_n X_{n-1} + b_{n-1} X_n}{X_n - X_{n-1}}. \tag{2}$$

PTO is achieved through damping devices installed along the hinges.

Assuming a potential flow, there exists a velocity potential $\boldsymbol{\Phi}$ satisfying the Laplace's equation $\nabla^2 \boldsymbol{\Phi} = 0$. In time-harmonic flows, the temporal dependence can be separated and $\boldsymbol{\Phi}$ is expressed as

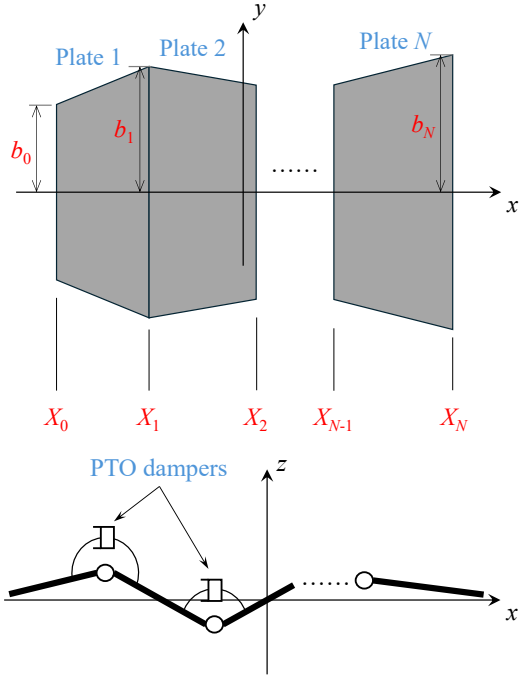

Figure 1 Schematic of an articulated floating-plate system consisting of N plates connected by hinges.

https://doi.org/10.26599/OCEAN.2026.9470020

$$\boldsymbol{\Phi}(x,y,z,t) = Re[\phi(x,y,z)e^{-i\omega t}], \tag{3}$$

where t denotes time, and ω is the angular frequency. Within the linear framework, the spatial potential ϕ can be decomposed as follows [31]:

$$\phi = \phi_I + \phi_S + \phi_R, \tag{4}$$

where ϕ_I, ϕ_S, and ϕ_R, denote the incident-wave, scattering, and radiation potentials, respectively. The diffraction potential is then written as $\phi_D = \phi_I + \phi_S$ and the incident-wave potential is written as [31]

$$\phi_I = -\frac{igA}{\omega} Z(z) e^{ik_0(x\cos\beta + y\sin\beta)}, \tag{5}$$

where A denotes the incident-wave amplitude, g denotes gravitational acceleration, and β is the wave heading angle with respect to the positive x-axis. In Eq. 5, $Z(z)$ is the vertical mode function written as

$$Z(z) = \begin{cases} e^{k_0 z} & \text{in deep water,} \\ \dfrac{\cosh[k_0(z+h)]}{\cosh(k_0 h)} & \text{in finite water depth,} \end{cases} \tag{6}$$

where k_0 is the wavenumber satisfying the dispersion relation $\omega^2 = gk_0$ in deep water and $\omega^2 = gk_0 \tanh(k_0 h)$ at finite water depth. Here, the deep-water wavenumber is defined as $K = \omega^2/g$. In the limit $h \to \infty$, we have $k_0 = K$.

The following kinematic and dynamic conditions are satisfied on the lower side of the floating plate:

$$\frac{\partial \phi}{\partial z} = -i\omega w \tag{7}$$

and

$$p = \underbrace{i\omega\rho\phi}_{p^{dyn}} \underbrace{-\rho g w}_{p^{sta}}, \tag{8}$$

where ρ is the water density.

3 Hydrodynamic analysis

The boundary-value problem outlined in Section 2 is solved using the boundary element method (BEM). This study uses two alternative boundary-integral formulations: the potential and pressure formulations.

3.1 Potential formulation

The potential formulation applies the boundary-integral equation directly to the velocity potential on the floating-plate surface:

$$4\pi\phi(\boldsymbol{x}) - K\iint_S \phi(\boldsymbol{x}')G(\boldsymbol{x},\boldsymbol{x}')dS = -\iint_S \frac{\partial\phi(\boldsymbol{x}')}{\partial z'} G(\boldsymbol{x},\boldsymbol{x}')dS, \tag{9}$$

where $\boldsymbol{x} = (x,y,z)$ and $\boldsymbol{x}' = (x',y',z')$ denote the field and source points, respectively, S is the lower wetted surface of the floating plate, and $G(\boldsymbol{x},\boldsymbol{x}')$ is the free-surface Green function that satisfies the linear free-surface boundary condition and the radiation condition [32,33]. This study adopts the free-surface condition $\partial_z G = KG$, where $K = \omega^2/g$. Because the floating plate has a small draft, the boundary-integral equation (Eq. 9) contains no irregular frequencies [34].

The unknown in Eq. 9 is either the scattering potential ϕ_S or the radiation potential ϕ_R. The vertical derivative of the potential (right-hand side of Eq. 9) is determined by the body boundary condition. In the diffraction problem, the body boundary condition is expressed as

$$\frac{\partial\phi_S}{\partial z} = -\frac{\partial\phi_I}{\partial z}, \tag{10}$$

where ϕ_I denotes the incident-wave potential given by Eq. 5.

The radiation problem decomposes the radiation potential into a sum of motion modes

$$\phi_R = -i\omega\sum_m X_m\phi_m, \tag{11}$$

where X_m is the complex motion amplitude in mode m, and ϕ_m is the corresponding potential per unit velocity. Based on the kinematic boundary condition given by Eq. 7, ϕ_m satisfies the following body boundary condition:

$$\frac{\partial\phi_m}{\partial z} = w_m(x), \tag{12}$$

where $w_m(x)$ is the generalized-mode function [35], defined as

$$w_m(x) = \begin{cases} 1 & m = 0, \\ |x - x_m| & 1 \le m \le N-1, \\ x & m = N. \end{cases} \tag{13}$$

Figure 2 illustrates the generalized modes of a three-hinged plate.

3.2 Pressure formulation

Combining the kinematic and dynamic conditions on the floating-plate surface, Eq. 9 can be reformulated as a boundary-integral equation in terms of *total* pressure. As described in Ref. [36], the boundary-integral equation is then reformulated as

$$p_D(\boldsymbol{x}) - \frac{K}{4\pi}\iint_S p_D(\boldsymbol{x}')G(\boldsymbol{x},\boldsymbol{x}')dS = i\omega\rho\phi_I(\boldsymbol{x}) \tag{14}$$

for the diffraction problem, and

$$p_m(\boldsymbol{x}) - \frac{K}{4\pi}\iint_S p_m(\boldsymbol{x}')G(\boldsymbol{x},\boldsymbol{x}')dS = -\rho g w_m(\boldsymbol{x}) \tag{15}$$

for the radiation problem.

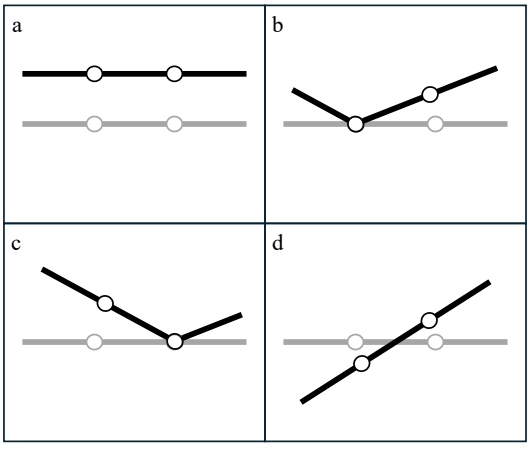

Figure 2 Generalized modes of three interconnected plates: (a) heave mode; (b) and (c) generalized tent modes; (d) pitch mode.

3.3 Hydrodynamic loads

The hydrodynamic loads acting on the floating plates arise from both the radiation generated by the wave motion and the diffraction of incident waves. The added mass A_{mn} and wave-radiation damping B_{mn} satisfy

$$A_{mn}+\mathrm{i}\,\omega B_{mn}=\frac{1}{\omega^2}\iint_S p_n^{\mathrm{dyn}}\,w_m\,\mathrm{d}S=\rho\iint_S \phi_n\,w_m\,\mathrm{d}S. \tag{16}$$

Likewise, the wave-excitation force associated with wave diffraction in mode m is

$$F_m^{\mathrm{ex}}=\iint_S p_{\mathrm{D}}\,w_m\,\mathrm{d}S=-\mathrm{i}\,\rho\,\omega\iint_S(\phi_{\mathrm{I}}+\phi_{\mathrm{S}})\,w_m\,\mathrm{d}S. \tag{17}$$

4 Wave-energy harnessing

The incident-wave energy is converted to useful power through the relative motions of the hinged plates, which drive the PTO dampers installed at the joint locations. The hydrodynamic response of the system is governed by the following coupled motion equation:

$$\boldsymbol{Z}\,\boldsymbol{U}-\boldsymbol{F}^{\mathrm{PTO}}=\boldsymbol{F}^{\mathrm{ex}}, \tag{18}$$

where $\boldsymbol{U}$ denotes the complex velocity vector associated with each generalized mode, and $\boldsymbol{Z}$ represents the combined hydrodynamic impedance defined as

$$\boldsymbol{Z}=\boldsymbol{B}-\mathrm{i}\,\omega\,(\boldsymbol{M}+\boldsymbol{A}-\frac{\boldsymbol{C}}{\omega^2}). \tag{19}$$

Here, $\boldsymbol{M}$ denotes the mass matrix, and $\boldsymbol{C}$ is the hydrostatic restoring matrix. The PTO mechanism imparts a force

$$\boldsymbol{F}^{\mathrm{PTO}}=-\boldsymbol{D}\,\boldsymbol{U}, \tag{20}$$

with $\boldsymbol{D}$ being a diagonal damping matrix defined as

$$\boldsymbol{D}=\mathrm{diag}(0,\lambda_1,\lambda_2,\ldots,\lambda_{N-1},0). \tag{21}$$

$\boldsymbol{D}$ reflects the absence of PTO actuation in rigid-body modes.

In Eq. 19, the elements of the mass matrix $\boldsymbol{M}$ and the hydrostatic restoring matrix $\boldsymbol{C}$ respectively take the classical forms [35]

$$M_{mn}=m_u\iint_S w_m(x)\,w_n(x)\,\mathrm{d}S, \tag{22}$$

$$C_{mn}=\rho g\iint_S w_m(x)\,w_n(x)\,\mathrm{d}S, \tag{23}$$

where w_m and w_n are mode-shape functions associated with the hinged-plate motions.

Wave power is harnessed through the hydrodynamic force, which comprises both the wave-excitation force and the radiation force:

$$\boldsymbol{F}^{\mathrm{dyn}}=\boldsymbol{F}^{\mathrm{ex}}+(\mathrm{i}\,\omega\boldsymbol{A}-\boldsymbol{B})\,\boldsymbol{U}. \tag{24}$$

The corresponding time-averaged power absorbed by the PTO system is

$$\begin{aligned}W&=\frac{1}{2}\,Re\{[\boldsymbol{F}^{\mathrm{dyn}}]^{\dagger}\,\boldsymbol{U}\}\\&=\frac{1}{2}\,\boldsymbol{U}^{\dagger}\,\boldsymbol{D}\,\boldsymbol{U}\\&=\frac{1}{2}\,[\boldsymbol{F}^{\mathrm{ex}}]^{\dagger}\,[(\boldsymbol{Z}+\boldsymbol{D})^{-1}]^{\dagger}\,\boldsymbol{D}\,(\boldsymbol{Z}+\boldsymbol{D})^{-1}\,\boldsymbol{F}^{\mathrm{ex}},\end{aligned} \tag{25}$$

where $(\cdot)^{\dagger}$ denotes the Hermitian transpose. As indicated by these expressions, power absorption is maximized when the PTO impedance is appropriately matched to the hydrodynamic response.

Following the block-matrix inversion approach of Ref. [37], the absorbed power is rewritten as

$$W=\frac{1}{2}\boldsymbol{f}^{\dagger}\,(\boldsymbol{Y}^{\dagger}+\boldsymbol{\Lambda})^{-1}\boldsymbol{\Lambda}\,(\boldsymbol{Y}+\boldsymbol{\Lambda})^{-1}\boldsymbol{f}, \tag{26}$$

where

$$\boldsymbol{\Lambda}=\mathrm{diag}(\lambda_1,\lambda_2,\cdots,\lambda_{N-1}). \tag{27}$$

The reduced impedance matrix $\boldsymbol{Y}=[Y_{nm}]$ and modified excitation vector $\boldsymbol{f}=\{f_n\}$ are respectively defined as

$$Y_{nm}=Z_{nm}-\frac{Z_{0n}\,Z_{0m}}{Z_{00}}-\frac{Z_{nN}\,Z_{mN}}{Z_{NN}},\quad \text{for } n,m=1,2,\cdots,N-1, \tag{28}$$

$$f_n=F_n^{\mathrm{ex}}-\frac{Z_{0n}}{Z_{00}}\,F_0^{\mathrm{ex}}-\frac{Z_{nN}}{Z_{NN}}\,F_N^{\mathrm{ex}},\quad \text{for } n=1,2,\cdots,N-1. \tag{29}$$

In this formulation, only the internal deformation modes contribute to energy capture.

In a system consisting of two hinged plates, only one internal mode contributes to power absorption. The time-averaged extracted power then reduces to

$$W=\frac{1}{2}\,\frac{\lambda_1\,|f_1|^2}{|Y_{11}+\lambda_1|^2}. \tag{30}$$

The present study considers a configuration of two hinged plates, the simplest articulated system allowing a closed-form solution of the optimal PTO damping and the corresponding wave-power extraction. In systems with more than two hinged plates, hydrodynamic coupling between multiple hinged modes leads to a fully coupled impedance matrix and a closed-form solution becomes mathematically intractable. Noad and Porter [38] showed that an exact analytical solution is unavailable for a configuration composed of three-hinged plates. Instead, they obtained the ranges for optimal PTO damping.

Equation 30 indicates a trade-off between PTO damping and hydrodynamic impedance. The energy extraction is optimized when the PTO damping coefficient is tuned to $\lambda_1=|Y_{11}|$. Under this impedance-matching condition, the optimal absorbed wave power is [37]

$$W_{\mathrm{opt}}=\frac{|f_1|^2}{4\,[Re(Y_{11})+|Y_{11}|]}. \tag{31}$$

The theoretical upper bound

$$W_{\mathrm{max}}=\frac{|f_1|^2}{8\,Re(Y_{11})} \tag{32}$$

is attained when the hydrodynamic impedance becomes purely real, i.e., $\mathrm{Im}(Y_{11})=0$.

To assess the performance of the system, the extracted power is normalized by the incident-wave energy flux per unit width [31]

$$W_{\mathrm{inc}}=\frac{\rho g A^2}{2}\,c_g,\quad \text{with}\quad c_g=\frac{\omega}{2k_0}\left[1+\frac{2k_0h}{\sinh(2k_0h)}\right]. \tag{33}$$

The non-dimensional capture factors are then given as

https://doi.org/10.26599/OCEAN.2026.9470020

$$\{\eta_{\text{opt}}, \eta_{\text{max}}\} = \frac{k_0\{W_{\text{opt}}, W_{\text{max}}\}}{W_{\text{inc}}}. \quad (34)$$

Here, the optimal wave power refers to the best achievable energy extraction under a given wave condition and structural hydrodynamic response. The wave power is optimized by tuning the PTO damping to match the magnitude of the complex hydrodynamic impedance. The theoretical upper bound, in which the hydrodynamic impedance becomes purely real, corresponds to the maximum wave power harnessed when the wave-excitation force and structural velocity are perfectly in phase.

5 Results and discussion

Before presenting the main results of the hinged-plate array, we validate the accuracy of the developed numerical model by comparing the predicted wave-induced motions of a single rectangular floating plate with the experimental measurements reported in [39].

The numerical-model setup is consistent with the experimental configuration. The length and width of the rectangular plate are $2a = 2.318$ m and $2b = 0.86$ m, respectively, and the test-water depth is $h = 3.0$ m. The surface density of the plate is uniform and given by $m_u = 42$ kg m^{-2}. Figure 3 plots the heave and pitch response amplitude operators of the plate versus non-dimensional wavenumber k_0a. The results of the potential and pressure formulations are almost identical, confirming the numerical consistency. Moreover, both sets of numerical results follow the experimental data across the entire range of wavenumbers. This close match demonstrates the accuracy and reliability of the present boundary-element implementation of single floating plates.

To further validate the generalized-mode model of hinged multi-body systems, we consider the motion response of a rectangular two-segment floating plate with an aspect ratio of $a/b = 2$. The hinge is located at the mid-length position ($x_1 = 0$). The hydrodynamic problem is solved through two independent numerical implementations: the generalized-mode formulation described in Section 2 with two rigid modes (heave and pitch) plus the "tent" mode, and the Lagrange multiplier method that enforces continuous vertical displacement at the hinge through constraint equations. Liang and Chen [36] validated the latter approach against the benchmark results of Ref. [40].

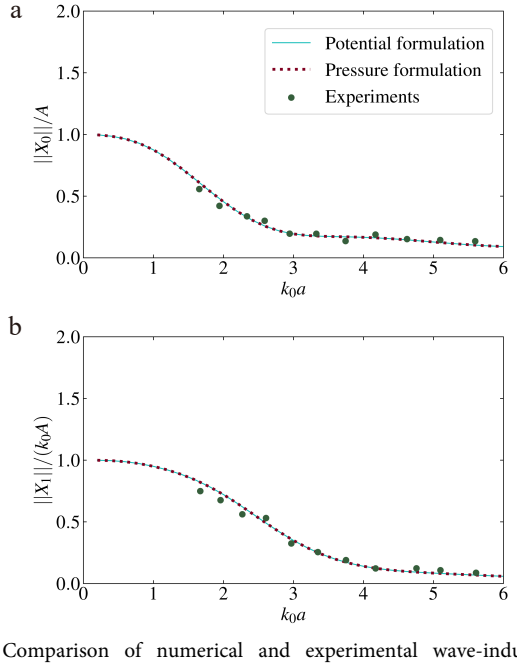

Figure 3 Comparison of numerical and experimental wave-induced motions of a floating rectangular plate: (a) heave motion X_0 and (b) pitch motion X_1. Comparison is made with the experimental results from Ref. [39].

Figure 4 shows the non-dimensional amplitudes of vertical motion and relative rotation at the hinge obtained from the generalized-mode and Lagrange multiplier formulations. Both sets of results coincide across the entire frequency range, demonstrating the high numerical consistency between the two methods. At low frequencies ($Ka \to 0$), the two segments move almost as a single rigid body with negligible relative rotation. As the frequency increases, the hinge mode is progressively excited and both the vertical motion and relative rotation exhibit pronounced peaks near $Ka \approx 2$, indicating the excitation of a strong flexural response at wavelengths comparable to the plate length. This satisfactory agreement confirms the robustness of the present generalized-mode implementation for articulated floating structures, laying the groundwork for the power-absorption analysis.

The generalized-mode approach directly uses the natural modes of the system, compactly representing its hinged-body motions, inherently satisfying the kinematic constraints, and reducing the computational cost. In contrast, the Lagrange multiplier method includes additional equations for the constraints, allowing straightforward handling of complex constraints. Overall, the generalized-mode method is more efficient than the Lagrange method and provides inherent mode insight, whereas the Lagrange multiplier technique is flexible and straightforward.

We now examine wave-energy extraction from a rectangular floating plate with an aspect ratio of $a/b = 2$. The plate, consisting of two segments joined by a single hinge located at $x = x_1$, is deployed in deep water. The plate is assumed to be uniformly thick with a mass distribution of $m_u = 500$ kg m^{-2}. Power is harnessed through a linear PTO system installed at the hinge.

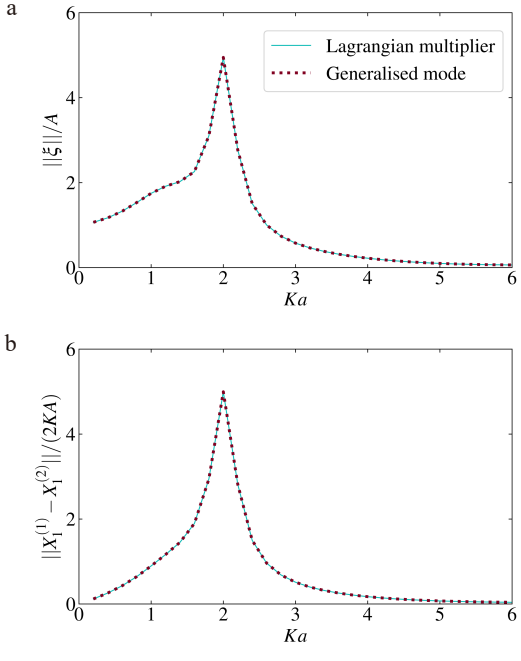

Figure 4 Motion responses at the hinge of a two-segment floating plate: (a) vertical motion and (b) relative rotational motion.

The contour plot in Fig. 5 shows the amplitude response of the tent mode, which is associated with wave-energy harnessing. The motion response peaks near $k_0a \approx 2.0$. The maximum response amplitude decreases monotonically as the hinge location shifts from the upwave toward the downwave side, demonstrating an important role of hinge placement in the energy extraction.

The contour plot in Fig. 6 shows the distribution of the normalized imaginary part of the intrinsic mechanical admittance of the hinge mode, $\mathrm{Im}[Y_{11}]/B_{11}$, as the non-dimensional wavenumber ka and relative hinge position x_1/a are varied. The locus of $\mathrm{Im}[Y_{11}] = 0$ is also plotted (solid black line). According to linear wave-energy theory, the power absorption is maximized by tuning the PTO damping until the imaginary part of the total admittance at the hinge vanishes (meeting the optimal impedance-matching condition). Therefore, the zero-crossing curve identifies the hinge location at which the energy extraction from the two-segment system is theoretically maximized at each wavenumber.

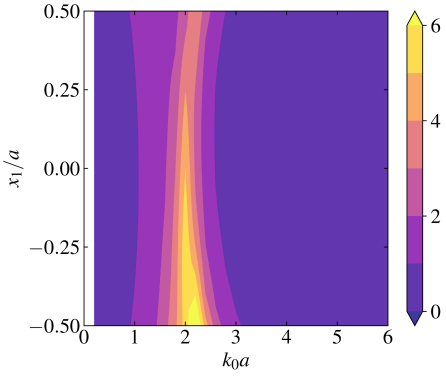

Figure 5 Amplitude response of the tent mode to non-dimensional wavenumber k_0a and hinge lcoation x_1/a.

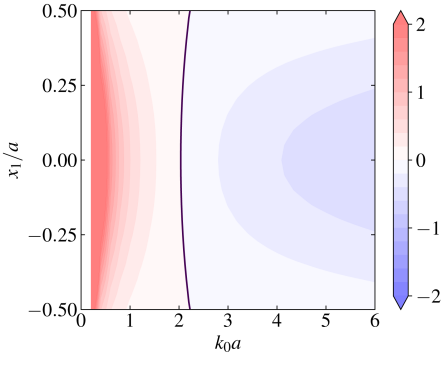

Figure 6 Distribution of $\mathrm{Im}[Y_{11}]/B_{11}$ in the k_0a–x_1/a plane. The solid line represents the zero crossing at which the wave-energy extraction is maximized.

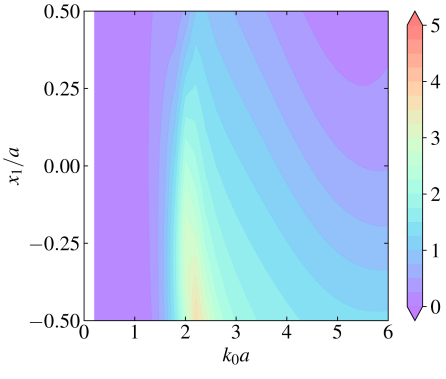

Figure 7 Distribution of non-dimensional wave-energy extraction η_{opt} in the k_0a–x_1/a plane.

The contour plot in Fig. 7 presents the corresponding optimal non-dimensional power-absorption efficiency η_{opt}, defined by Eq. 34, as k_0a and x_1/a are varied. A pronounced ridge of high absorption on the efficiency surface exactly follows the zero-crossing line of $\mathrm{Im}[Y_{11}]$ in Fig. 6, confirming the close link between the intrinsic hydrodynamic properties and maximum achievable performance of the hinged structure.

The plot is remarkably asymmetric with respect to hinge position. Moving the hinge toward the upwave (leading) edge ($x_1/a < 0$) increases the peak values of the tent-mode amplitudes, as illustrated in Fig. 5. Such enhancement translates to a remarkable increase in wave-energy extraction, appreciably enhancing the absorption over a wide frequency band. In comparison, placing the hinge toward the downwave (trailing) edge ($x_1/a > 0$) suppresses the energy-extraction performance and the optimal capture factor η_{opt} decreases over most of the spectrum. The sensitivity of hinge location highlights the importance of positioning the power take-off near the incident-wave side, where the vertical motion amplitude and hence the relative rotation about the hinge are large. This configuration maximizes the energy available for extraction.

6 Concluding remarks

A hydrodynamic analysis of an articulated floating-plate WEC was implemented in a BEM with generalized modes, which efficiently models the hinged structure. Potential and pressure formulations of the boundary-integral yielded consistent results, both validated against experimental and benchmark results.

Hinge position was found to play an essential role in optimizing the power absorption of a two-segment raft. When the hinge is asymmetrically placed toward the upwave side, the capture efficiency is enhanced above unity over a broad frequency range. Aligning the hinge locus with the zero-impedance condition considerably enhances the performance without adding structural complexity. Moreover, the generalized-mode approach is computationally scalable to multi-segment devices.

The applicability of this research extends beyond wave-power absorption to studies of other marine structures such as floating solar farms and breakwaters. We also plan to adapt the chain-type hinge into a mesh layout in future work.

The present study is not without limitations. The hydrodynamic analysis assumed linear potential flow theory, which neglects viscous effects and nonlinear wave–structure interactions. The latter are important for large-amplitude motions in high sea states.

Acknowledgements

None.

Author contribution statement

H.L.: Conceptualization, Formal analysis, Investigation, Methodology, Validation, Visualization, Writing - original draft, Writing - review & editing; S.Z.: Conceptualization, Investigation, Funding acquisition, Writing - review & editing; H.C.: Conceptualization, Formal analysis, Writing - review & editing. All the authors have approved the final manuscript.

Data availability

The data that support the findings of this study are available from the corresponding author upon reasonable request.

Declaration of competing interest

All the contributing authors report no conflicts of interest in this work.

Funding

This work is supported by National Key R&D Program of China (Grant No. 2024YFB4207000 to S.Z.).

Use of AI statement

None.

References

[1] Iglesias, G., Carballo, R. (2010). Offshore and inshore wave energy assessment: Asturias (N Spain). *Energy* 35, 1964–1972.

[2] Iglesias, G., Carballo, R. (2011). Choosing the site for the first wave farm in a region: a case study in the Galician Southwest (Spain). *Energy* 36, 5525–5531.

[3] Neill, S. P., Lewis, M. J., Hashemi, M. R., Slater, E., Lawrence, J., Spall, S. A. (2014). Inter-annual and inter-seasonal variability of the Orkney wave power resource. *Appl. Energy* 132, 339–348.

[4] Reguero, B. G., Losada, I. J., Méndez, F. J. (2015). A global wave power resource and its seasonal, interannual and long-term variability. *Appl. Energy* 148, 366–380.

[5] Drew, B., Plummer, A. R., Sahinkaya, M. N. (2009). A review of wave energy converter technology. *Proc. Inst Mech. Eng. Part A J. Power Energy* 223, 887–902.

[6] Zheng, S. M. (2022). Attenuator wave energy converters. In Modelling and Optimization of Wave Energy Converters. Ning, D. Z., Ding, B. Y., Eds. Boca Raton: CRC Press.

[7] Haren, P., Mei, C. C. (1979). Wave power extraction by a train of rafts: hydrodynamic theory and optimum design. *Appl. Ocean Res.* 1, 147–157.

[8] McCormick, M. E., Murthagh, J., McCab, P. (1998). Large-scale experimental study of a hinged-barge wave energy conversion system. In *Proceedings of the 3rd European Wave Energy Conference Patras*. Greece, p 215–222.

[9] Yemm, R., Pizer, D., Retzler, C., Henderson, R. (2012). Pelamis: experience from concept to connection. *Philos. Trans. Roy. Soc. A Math. Phys. Eng. Sci.* 370, 365–380.

[10] Zanuttigh, B., Martinelli, L., Castagnetti, M., Ruol, P., Kofoed, J. P., Frigaard, P. (2010). Integration of wave energy converters into coastal protection schemes. In *Proceedings of the 3rd International Conference and Exhibition on Ocean Energy*. Bilbao, p 1–6.

[11] LTD FE. (2015). Sea power wave energy converter. https://foynesengineering.wearetherift.com/our_proje.

[12] Carpintero Moreno, E., Stansby, P. (2019). The 6-float wave energy converter M4: ocean basin tests giving capture width, response and energy yield for several sites. *Renew. Sustain. Energy Rev.* 104, 307–318.

[13] Mocean Energy. (2019). Green energy out of the blue. https://www.mocean.energy/#green-energy. (accessed 23 November 2025)

[14] Farley, F. J. M., Rainey, R. C. T. (2006). Anaconda: the bulge wave sea energy converter. Maritime Energy Development Ltd.

[15] Babarit, A., Singh, J., Mélis, C., Wattez, A., Jean, P. (2017). A linear numerical model for analysing the hydroelastic response of a flexible electroactive wave energy converter. *J. Fluids Struct.* 74, 356–384.

[16] Zheng, S. M., Zhang, Y. H., Zhang, Y. L., Sheng, W. A. (2015). Numerical study on the dynamics of a two-raft wave energy conversion device. *J. Fluids Struct.* 58, 271–290.

[17] Jin, S. Y., Wang, D. M., Hann, M., Collins, K., Conley, D., Greaves, D. (2023). A designed two-body hinged raft wave energy converter: from experimental study to annual power prediction for the EMEC site using WEC-Sim. *Ocean Eng.* 267, 113286.

[18] Han, Z., Jin, S. Y., Greaves, D., Hann, M., Shi, H. D. (2024). Study on the energy capture spectrum of a two-body hinged-raft wave energy converter. *Energy* 304, 132057.

[19] Zhang, J. C., Zhao, X. W., Greaves, D., Jin, S. Y. (2023). Modeling of a hinged-raft wave energy converter via deep operator learning and wave tank experiments. *Appl. Energy* 341, 121072.

[20] Zheng, S. M., Zhang, Y. L., Sheng, W. A. (2016). Maximum theoretical power absorption of connected floating bodies under motion constraints. *Appl. Ocean Res.* 58, 95–103.

[21] Zheng, S. M., Zhang, Y. L., Sheng, W. A. (2016). Maximum wave energy conversion by two interconnected floaters. *J. Energy Resour. Technol.* 138, 032004.

[22] Zheng, S. M., Zhang, Y. L. (2017). Analysis for wave power capture capacity of two interconnected floats in regular waves. *J. Fluids Struct.* 75, 158–173.

[23] Lu, D., Tian, X. L., Lu, W. Y., Zhang, X. T. (2019). Combined effects of raft length ratio and structural flexibility on power capture performance of an interconnected-two-raft wave energy converter. *Ocean Eng.* 177, 12–28.

[24] Zhang, H. C., Zhou, X., Xu, D. L., Zou, W. S., Ding, J., Xia, S. Y. (2022). Nonlinear stiffness mechanism for high-efficiency and broadband raft-type wave energy converters. *Mech. Syst. Signal Process.* 177, 109168.

[25] Abbasi, A., Ghassemi, H. (2024). Numerical results of the dynamic response and capture factor of the two-raft-type WEC. *Energy Convers. Manage.* 303, 118176.

[26] Wan, C., Yang, C., He, M., Baldock, T. E., Nielsen, P., Johanning, L. (2025). Hydrodynamic and power conversion performance of a hybrid raft-type WEC and breakwater system using SPH method. *Renew. Energy* 245, 122753.

[27] He, K. D., Gao, H. T. (2025). Wave-to-wire simulation of a raft-type WEC with a mechanical PTO. *Ocean Eng.* 341, 122629.

[28] Wang, L. G., Wen, C. W., Wu, S. X., Wu, S. (2024). Electric power prediction of a two-body hinge-barge wave energy converter using machine learning techniques. *Ocean Eng.* 305, 117935.

[29] Liu, C. H., Yang, Q. J., Bao, G. (2018). Latching control using optimal control method for a raft-type wave energy converter. *Ships Offshore Struct.* 13, 138–154.

[30] Cheng, Y., Liu, W. F., Dai, S. S., Yuan, Z. M., Incecik, A. (2024). Wave energy conversion by multi-mode exciting wave energy converters arrayed around a floating platform. *Energy* 313, 133621.

[31] Newman, J. N. (1977). Marine Hydrodynamics. Cambridge: MIT Press.

[32] Wehausen, J. V., Laitone, E. V. (1960). Surface waves. In Fluid Dynamics / Strömungsmechanik. Truesdell, C., Ed. Berlin: Springer, p 446–778.

[33] Linton, C. M., McIver, P. (2001). Handbook of Mathematical Techniques for Wave/Structure Interactions. New York: Chapman and Hall/CRC.

[34] Liang, H., Ouled Housseine, C., Chen, X. B., Shao, Y. L. (2020). Efficient methods free of irregular frequencies in wave and solid/porous structure interactions. *J. Fluids Struct.* 98, 103130.

[35] Newman, J. N. (1994). Wave effects on deformable bodies. *Appl. Ocean Res.* 16, 47–59.

[36] Liang, H., Chen, X. B. (2025). Boundary element method for wave interactions with marine structures: from conventional to emerging applications. *Eng. Anal. Boundary Elem.* 179, 106326.

[37] Noad, I. F., Porter, R. (2017). Modelling an articulated raft wave energy converter. *Renew. Energy* 114, 1146–1159.

[38] Noad, I. F., Porter, R. (2015). Optimisation of arrays of flap-type oscillating wave surge converters. *Appl. Ocean Res.* 50, 237–253.

[39] Michele, S., Zheng, S., Renzi, E., Guichard, J., Borthwick, A. G. L., Greaves, D. M. (2024). Wave energy extraction from rigid rectangular compound floating plates. *J. Fluids Struct.* 130, 104193.

[40] Sun, L., Eatock Taylor, R., Choo, Y. S. (2011). Responses of interconnected floating bodies. *IES J. Part A Civil Struct. Eng.* 4, 143–156.